

FACILE SCALABLE SYNTHESIS OF SiOC/CARBON NANOHYBRIDS AS LITHIUM-ION BATTERY ANODE INSPIRED BY DENTAL RESTORATIVE MATERIALS

M. WANG^{a,b}, Y. XIA^a, X. WANG^{a,c}, Y. XIAO^a, Q. ZHANG^a, R. LIU^d, B. QIU^a,
Q. WU^e, G. CHEN^a, Y. LIU^a, Z. YANG^e, Z. LIU^a, J.Q. MENG^c, L.D. SUN^d,
C. H. YAN^d, J. PAN^b, Y. J. CHENG^{a*}

^a*Ningbo Institute of Materials Technology and Engineering, Chinese Academy of Sciences, 1219 Zhongguan West Rd, Zhenhai District, Ningbo, Zhejiang Province 315201, P. R. China*

^b*Faculty of Materials Science and Chemical Engineering, Ningbo University, Ningbo, Zhejiang Province 315211, P. R. China*

^c*State Key Laboratory of Separation Membranes and Membrane Processes, Tianjin Polytechnic University, Tianjin 300387, P. R. China*

^d*Beijing National Laboratory for Molecular Sciences, State Key Laboratory of Rare Earth Materials Chemistry and Applications & PKU-HKU Joint Lab on Rare Earth Materials and Bioinorganic Chemistry, College of Chemistry and Molecular Engineering, Peking University, Beijing 100871, P. R. China*

^e*Soochow University, Center for Soft Condensed Matter Physics & Interdisciplinary Research, Suzhou 215006, P. R. China*

A facile scalable strategy inspired by dental restorative methacrylates has been developed to synthesize SiOC/C nanohybrids. Great flexibility to tune the content and microstructure of the free carbon matrix has been achieved by varying the amount of the methacryloxypropylmethyldimethoxysilane (MPDMS) incorporated into the cross-linked methacrylate network. Good electrochemical performance as lithium-ion battery anode has been observed.

(Received January 28, 2016; Accepted May 23, 2016)

Keywords: Energy Storage; Silicon Oxycarbide; Nanohybrids; Methacrylate;
Lithium-Ion Battery Anode

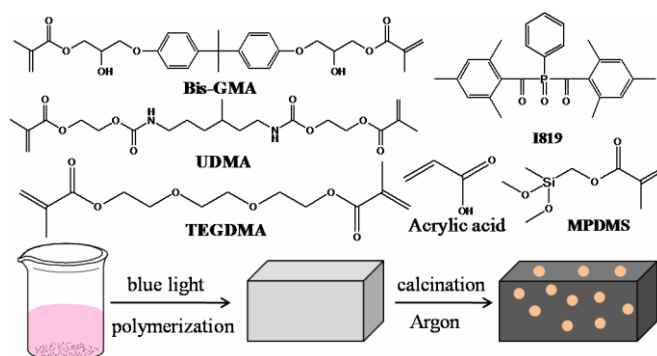
1. Introduction

The last two decades have witnessed a great success of rechargeable lithium-ion batteries (LIBs) in portable electronic devices, electric vehicles, and energy storage[1-4]. However, inferior capacity and serious safety risk of the commercialized graphite anode have dramatically limited wide applications of the LIBs. Searching for next-generation LIB anode with superior specific

*Corresponding author: chengyj@nimte.ac.cn

capacity, attractive voltage profile, excellent cyclic stability, outstanding rate performance, and reliable operation safety has received tremendous attention[5, 6].

Polymer derived ceramics (PDCs) such as silicon oxycarbide (SiOC) glasses have gained renewed interest as alternative LIB anodes following extensive research work in the 1990s, due to high reversible capacities, good cyclic stability, and possible commercialization plan by Dow Corning[7-11]. Within the SiOC phase, silicon atoms bond to oxygen and carbon atoms to form $\text{SiO}_x\text{C}_{4-x}$ tetrahedral structures[12]. Besides, free carbon usually coexists with the SiOC. The exact mechanism for the unique electrochemical properties of the SiOC is not fully understood yet[9]. But it is commonly recognized that SiOC acts as stabilizer for the free carbon matrix, while the free carbon phase mainly contributes to the discharge/charge capacities. The structure and mutual interaction between the SiOC and free carbon network are crucial for the electrochemical performance as lithium-ion battery anode[13, 14]. Conventionally, SiOC glasses are synthesized via pyrolysis of polysiloxanes, while the amount of free carbon is adjusted by tuning the cross-linking degree of the polysiloxanes[15]. However, the extent of modifying the structure and interaction between the SiOC and free carbon network is rather limited. It is necessary to develop new methods to significantly broaden the scope of structure modification in order to achieve improved performance.



Scheme 1. Synthesis of SiOC/C nanohybrids and molecular structure of the resin monomers, silane coupling agent, and photo initiator.

Here we report a new strategy to synthesize SiOC glasses with great flexibility to tune microstructure and content of both SiOC and free carbon in a facile scalable way (**Scheme 1**). Inspired by polymeric dental materials, difunctional resin monomers including Bisphenol A glycerolate methacrylate (Bis-GMA), triethylene glycol dimethacrylate (TEGDMA) and urethane dimethacrylate (UDMA) are used as reaction medium and carbon source[16-18]. Silane coupling agent of methacryloxypropylmethyl dimethoxysilane (MPDMS) is used as the precursor for SiOC. Photo polymerization triggered by blue light illumination is applied to form cross-linking methacrylate-silane network. Via calcination in argon atmosphere, SiOC and free carbon are *in situ* formed to generate SiOC/carbon nanohybrids, where the amount and structures of the free carbon within the SiOC/C nanohybrids can be easily tuned.

Compared to the previously reported research work, the method developed by us has a few particular advantages. First, difunctional methacrylate monomers are used as main carbon source. It provides great flexibility to tune the amount and structure of free carbon. Second, small silane

molecules instead of polysiloxanes are used as the precursor for SiOC. They can be integrated into the cross-linked methacrylate network at molecular level by copolymerization, leading to the simultaneous *in situ* formation of SiOC and free carbon. Enhanced control over the structure of the SiOC/free carbon network is possible. Third, besides acting as carbon source, the difunctional methacrylate monomers are also used as solvent. No tedious, costly, and environmentally unfriendly solvent post-processing treatment is needed. Fourth, the photo polymerization is a fast, scalable, energy saving, and environmentally benign process [19, 20].

2. Experimental

2.1 Materials

All of the chemicals were used as received without further purification. Acrylic acid (AA) was purchased from Sinopharm Group Co., Ltd. Bisphenol A glycerolate methacrylate (Bis-GMA), urethane dimethacrylate (UDMA) and Triethylene glycol dimethacrylate (TEGDMA) were donated by Esstech, Inc., USA. Phenyl bis (2, 4, 6-trimethylbenzoyl) phosphine oxide (Irgacure 819 photo initiator) was purchased from Sigma-Aldrich. Methacryloxypropylmethyl dimethoxysilane (MPDMS) was purchased from Nanjing CHENGONG silicone materials Co. Ltd.

2.2 Sample Preparation and Characterization

Firstly, Bis-GMA, UDMA and TEGDMA were mixed together with the mass ratio of 4:6:4. Then I-819 (1% mass fraction) was dissolved in the resin mixture to obtain photo active B/U/T solution. MPDMS (0g to 4.0 g) was dissolved into the B/U/T solution. 2g of AA was then added to the solution, followed by stirring for around five minutes. The as-prepared solution was poured into a silicone rubber mould which was clamped between two glass slides afterwards. Thereafter, photo polymerization was conducted by illuminated with a visible light-curing unit (Luxomat D, blue light 9 W, range of emission: 350 nm - 500 nm) for 3 minutes each side. The solidified samples were then baked at 60°C for 24 hours. Then the samples were released from the moulds and cut into small particles by kitchen mixer. Calcination in argon was applied at 800 °C in argon atmosphere for 4 hours in tube furnace with a ramp rate of 5 °C /min starting from room temperature, followed by natural cooling to room temperature. After calcination, the SiOC/C powders were ball-milled by a planetary ball miller (FRITSCH- pulverisette 7, Germany) for 4 hours with the speed of 400 rpm before characterization and electrochemical performance test.

Field emission scanning electron microscopy (FESEM) images were obtained with Hitachi S4800 scanning electron microscope (Tokyo, Japan) at an accelerating voltage of 4 kV. Field emission scanning electron microscope (FESEM) EDX elemental mapping images were obtained with FEI QUANTA 250 FEG (America FEI) at an accelerating voltage of 15 kV.

The transmission electron microscopy (TEM) of the samples were recorded with JEOL JEM-2100F TEM or Tecnai F20 (America FEI) instrument operated at 200 kV.

Scanning transmission electron microscopy (STEM) was measured by Tecnai F20.

The crystallographic phases of the SiOC/C nanohybrids were investigated by X-ray diffraction (XRD) (Bruker AXS D8 Advance, $\lambda=1.541 \text{ \AA}$, 2.2 kW) with 2θ ranged from 5 ° to 90 °.

X-ray photoelectron spectroscopy (XPS) measurement was carried out with an ESCALAB 250Xi spectrometer, using focused mono chromatized Al K α radiation ($h\nu = 1486.6$ eV) at room temperature.

The content of carbon of the SiOC/C nanohybrids was studied by Thermo Gravimetric Analyzer (TGA, Mettler Toledo, Switzerland) with the temperature range from 50 °C to 800 °C with the ramp rate of 20 K/min in air.

Raman spectroscopy was collected on a Renishaw (in Via-reflex) with the wavelength of 532 nm.

2.3 Electrochemical Measurement

2032-type coin cells were employed to evaluate the electrochemical performance of SiOC/C nanohybrids as lithium ion battery anodes. A slurry mixture was prepared by dispersing active material, Super P and poly (vinylidene fluoride) (PVDF) (mass ratio: 8:1:1) in N-methyl Pyrrolidone (NMP). The electrodes were prepared by spreading the slurry mixture on a piece of copper foil, followed by drying at 80 °C in vacuum for 12 h. The copper foil was pressed and, then the laminates were punched into round discs with a diameter of 13 mm, followed by drying at 80 °C further for 4 hours.

Lithium foil was used as the counter electrode. Electrolyte (Dongguan shanshan battery material Co., LTD) was used, where 1.0 M LiPF₆ was dissolved in a mixture of ethylene carbonate (EC) and diethyl carbonate (DMC) (1:2 v/v). The rate performance was measured at the current density sequence of 0.1 C, 0.2 C, 0.5 C, 1.0 C, 2.0 C, 5.0 C, 10 C, 20 C, and 0.1 C in the voltage range between 3.0 V and 0.005 V (vs. Li/Li⁺) (five cycles each current density, 1 C = 500 mAh/g). The cyclic measurement was carried out at a current density of 0.2 C in the voltage range of 3.0 V – 0.005 V (vs. Li/Li⁺) for 50 rounds. The specific capacity was calculated on the basis of only the active material. The lithiation process was defined as discharging, while the delithiation process was expressed as charging.

Cyclic voltammetry (CV) test was performed on a CHI 1040B potentiostat/galvanostat analyzer (Shanghai Chenhua instrument Co., Ltd) at a scanning rate of 0.1 mV/s from 0.005 V – 3 V.

3. Results & Discussion

The TEM images in Fig. 1 shows that no distinct morphology of SiOC can be observed with respect to different amounts of MPDMS. SiOC is homogeneously distributed within the carbon matrix at molecular level. The variation of the MPDMS mass ratio does not significantly modify the structure of the SiOC/C nanohybrids. Selected area electron diffraction (SAED) results suggest that both the SiOC and free carbon are amorphous.

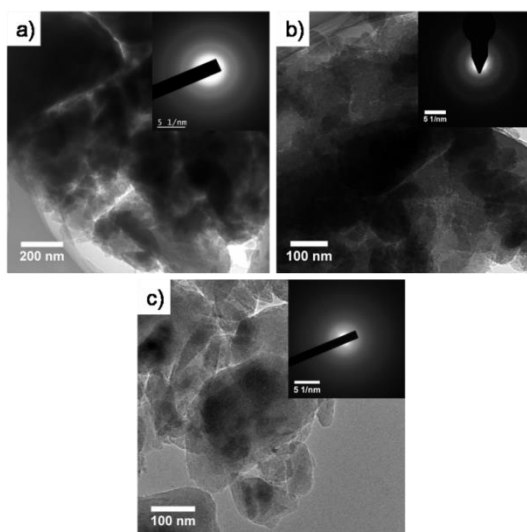


Fig. 1. TEM images of the SiOC/C nanohybrids prepared with different MPDMS mass ratios over the total mass of the resin monomer: (a) 0.125, (b) 0.50 and (c) 2.0. Insets: selected area electron diffraction (SAED) patterns of each TEM image.

According to the scanning transmission electron microscopy (STEM) images in Figure 2, the species of silicon, oxide and carbon are evenly distributed at nanometer scale in the region of $400 \text{ nm} \times 400 \text{ nm}$. While the carbon signal in the STEM image also includes the contribution from the carbon matrix, the homogeneous distribution of silicon and oxygen in the STEM image confirms the presence of SiOC at molecular level within the carbon matrix.

The scanning electron microscopy (SEM) images (Figure 3 and 4) show featureless structures at large size scale, which is consistent with the TEM images. Furthermore, the energy dispersive x-ray spectroscopy (EDX) images prove that SiOC are homogeneously distributed within the carbon matrix in the area with the size of over $10 \mu\text{m} \times 10 \mu\text{m}$ (Figure 5).

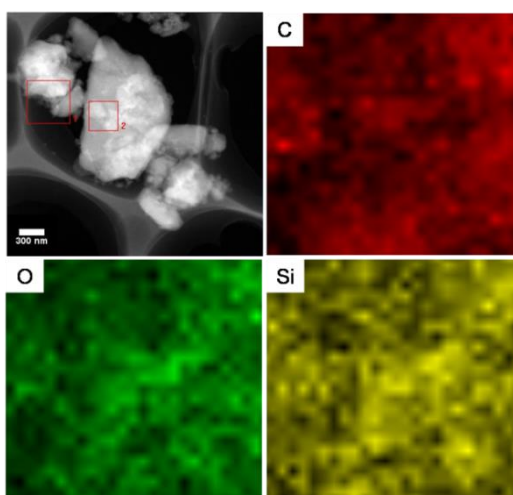


Fig. 2. STEM image of SiOC/C nanohybrids prepared with the MPDMS mass ratios of 0.50 over the total mass of the resin monomer. The box 1 is used as position reference and the box 2 is used as the region for elemental mapping.

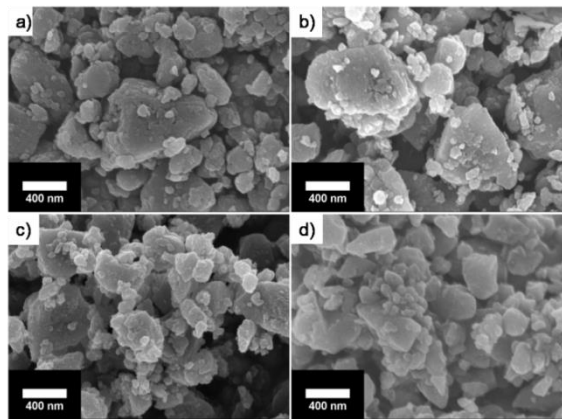


Fig. 3. High magnification SEM images of the SiOC/C nanohybrids prepared with different mass ratios of MPDMS over the total mass of the resin monomer: (a) 0, (b) 0.125, (c) 0.50 and (d) 2.0.

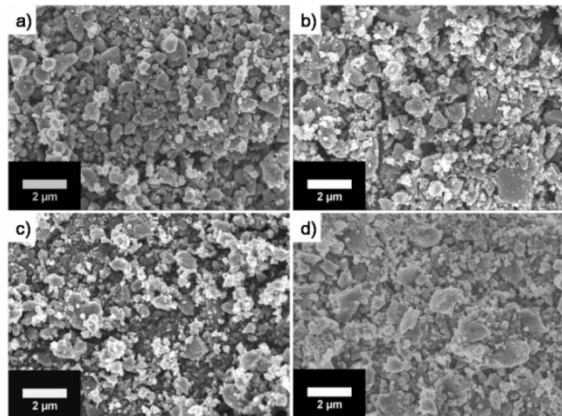


Fig. 4. Low magnification SEM images of the SiOC/C nanohybrids prepared with different mass ratios of MPDMS over the total mass of the resin monomer: (a) 0, (b) 0.125, (c) 0.50 and (d) 2.0.

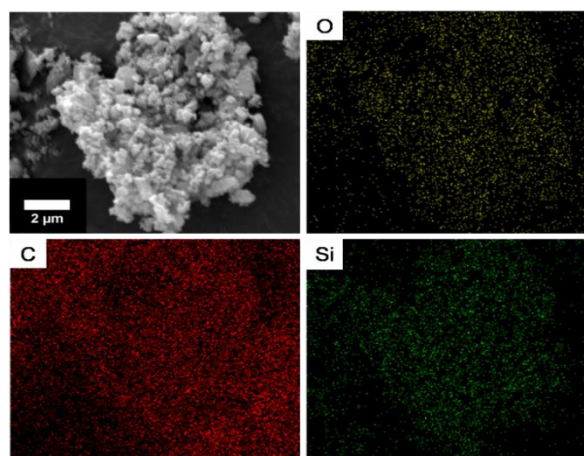


Fig. 5. EDX image of the SiOC/C nanohybrids prepared with mass ratios of MPDMS over the total mass of the resin monomer of 0.50.

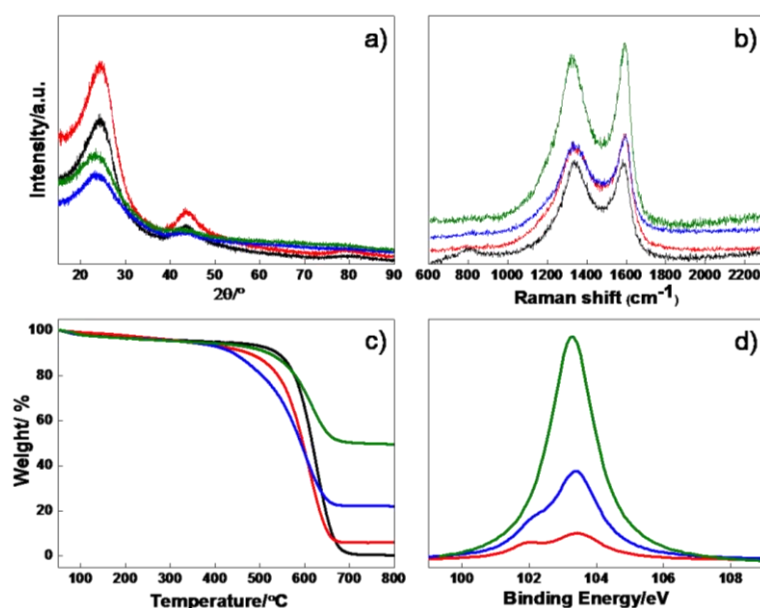


Fig. 6. XRD(a), Raman(b), TGA(c), and XPS(d) of the SiOC/C nanohybrids prepared with different mass ratios of MPDMS over the total mass of the resin monomer. Black: 0, Red: 0.125, Blue: 0.50, and Olive: 2.0.

The x-ray diffraction (XRD) pattern of the SiOC/C nanohybrid in Figure 6a further confirms that amorphous SiOC is formed, which is consistent with SAED. Furthermore, the presence of two broad peaks at 23.9° and 43.0° represents graphene sheets embedded in disordered carbon [7]. It is noticed that the SiOC/C nanohybrid prepared with the MPDMS mass ratio of 0.125 exhibits the most distinct peak located at 43.0° . It suggests that the incorporation of MPDMS with the mass ratio of 0.125 promotes the formation of both disordered and ordered (graphitic) carbon by enhancing the cross-linking degree of the methacrylate network. Because the diffractive signal from the disordered carbon mainly exists as background, the signal from the ordered carbon becomes distinct. With further increased amount of MPDMS, the copolymerization between MPDMS and resin monomers deteriorates the cross-linking degree and correspondingly the generation of graphitic carbon is inhibited. Therefore, the relative intensities of the peak at 43.0° are reduced with the MPDMS mass ratio of 0.50 and 2.0.

The Raman spectrum shows two peaks located at 1360 cm^{-1} (D band) and 1580 cm^{-1} (G band) (Figure 6b). The D band corresponds to the disorder-induced vibration of six-fold sp^2 -rings while the G band originates from an in-plane bond stretching of sp^2 -hybridized carbon atoms [21, 22]. In all spectra the integral intensities of the D band are more intense than those of the G band, which suggests that the disordered structure is overwhelming to the ordered carbon [13, 23]. Specifically, the bare carbon sample has the smallest D band peak width and lowest integral intensity ratio of I_D/I_G . With the MPDMS mass ratio of 0.125, the D band peak width and intensity ratio of I_D/I_G are increased [24]. It indicates that MPDMS enhances the cross-linking degree of the methacrylate network, promoting the formation of disordered carbon. The enhanced cross-linking is ascribed to the chemical reaction between the methoxyl-silane group of MPDMS and the hydroxyl group of the Bis-GMA and AA. Because each MPDMS molecule has two

methoxyl-silane functional groups, MPDMS acts as cross-linking center for the methacrylate network. However, with the MPDMS mass ratio further increased to 0.50 and 2.0, the D band peak width and intensity ratio of I_D/I_G decrease. The results suggest that the formation of disordered carbon compared to ordered carbon is reduced. Furthermore, the D band positions of the SiOC/C nanohybrids are shifted towards higher wavelength values with increasing MPDMS amount. The upward shift of the D band position also implies the increase of ordered carbon within the free carbon matrix[25]. With the MPDMS mass ratio increased to 0.50 and 2.0, the copolymerization between MPDMS and resin monomer comes to dominate. Because the copolymerization process decreases the overall cross-linking degree of the methacrylate network, less disordered carbon is formed.

With the MPDMS mass ratio increased from 0 to 2.0, the amount of free carbon content is decreased from 100 % to 94 %, 78 %, and 50 % respectively according to thermo gravimetric analyzer (TGA) (Figure 6c). The XPS spectroscopy shows that main peaks are located at about 103 eV typical for the Si-O bond (Figure 6d). With increasing amount of MPDMS, the peak position shifts from 103.5 eV to 103.3 eV, which suggests the formation of silicon-carbon bonding[26]. Besides, an additional shoulder peak located at about 102 eV exists, indicating the presence of $\text{SiO}_2\text{C}_{2[12]}$. The intensity of the shoulder peak gradually reduces with increasing amount of MPDMS. It is almost invisible with the MPDMS mass ratio of 2.0. The continuous decreasing shoulder peak intensity implies that the oxygen content within $\text{SiO}_x\text{C}_{4-x}$ is raised with increasing MPDMS content.

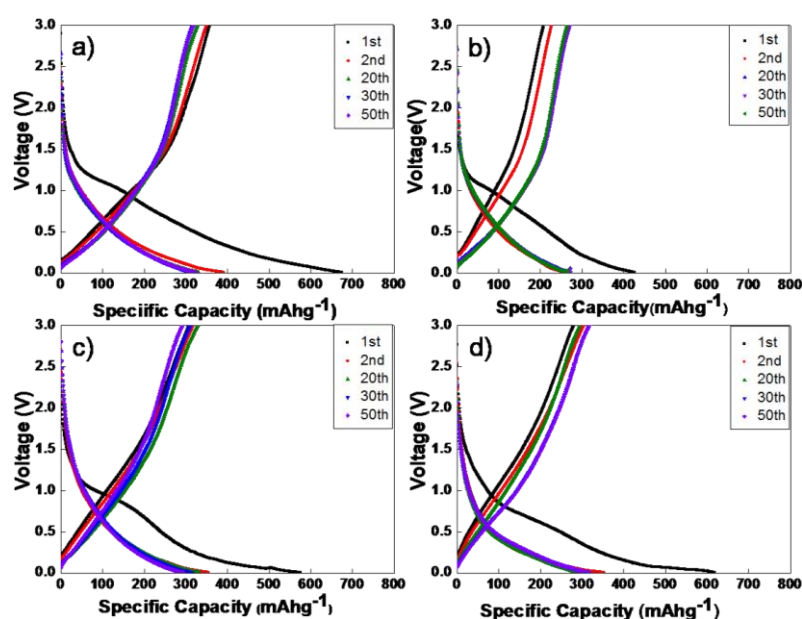


Fig. 7. Charge/discharge curves of the SiOC/C nanohybrids with different mass ratios of MPDMS over the total mass of the resin monomer: (a) 0, (b) 0.125, (c) 0.50 and (d) 2.0.

The discharge/charge curves of the SiOC/C nanohybrid anodes at the current density of 0.2 C ($1 \text{ C} = 500 \text{ mA g}^{-1}$) are exhibited in Fig. 7 and Fig. 8. Figure 4a shows typical discharge/charge curves of polymer pyrolyzed carbon. The initial discharge/charge capacities are

675 mAhg^{-1} and 357 mAhg^{-1} respectively, which are reduced to around 318 mAhg^{-1} after 50 cycles. With the MPDMS mass ratio increased to 0.125, 0.50, and 2.0, the initial discharge capacities are 426 mAhg^{-1} , 575 mAhg^{-1} and 618 mAhg^{-1} , while the initial charge capacities are 208 mAhg^{-1} , 308 mAhg^{-1} and 280 mAhg^{-1} respectively. After 50 cycles the capacities are around 267 mAhg^{-1} , 295 mAhg^{-1} and 318 mAhg^{-1} .

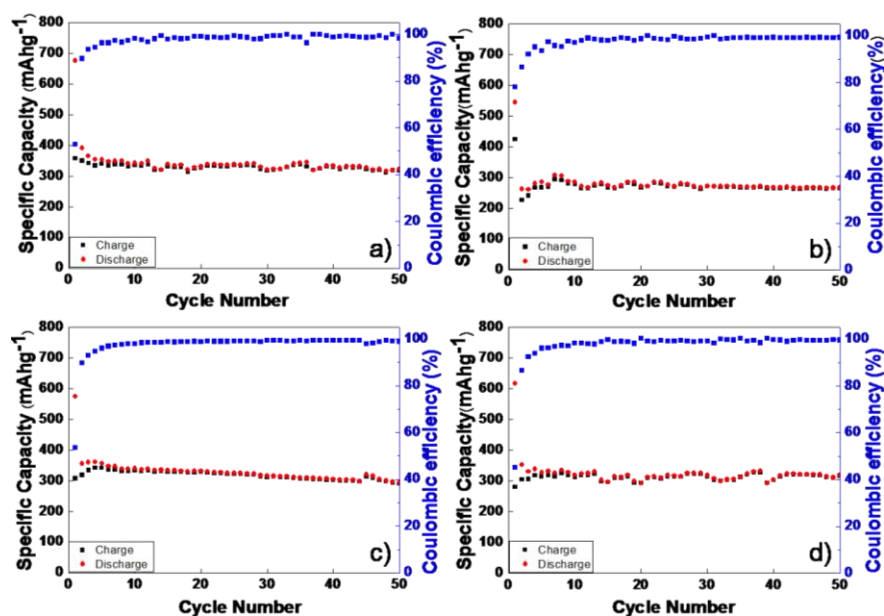


Fig. 8. Cyclic performance of the SiOC/C nanohybrids prepared with different mass ratios of MPDMS over the total mass of the resin monomer: (a) 0, (b) 0.125, (c) 0.50 and (d) 2.0.

The capacity loss from the first cycle is mainly due to formation of solid electrolyte interface (SEI), which is confirmed by the cyclic voltammetry test (Figure 9). The peak between 0.5V and 1V in the first cycle is ascribed to the formation of the SEI layers on the surface of the SiOC/C anode. From the second cycle there are no distinct peaks during the anodic and cathodic polarization processes, which is typical for bare carbon anode. The CV results indicate that it is the carbon phase which mainly involves in the lithiation/delithiation process. Compared to the bare carbon anode, the SiOC/C nanohybrids show similar performance with respect to the initial and cycled capacities. However, it should be pointed that the free carbon matrix acts as the major active sites for lithium intercalation and the SiOC phase is regarded as electrochemically inactive for lithiation [27]. If the mass of SiOC is excluded from the total mass of the active material, the calculated capacities of the free carbon matrix are quite high [27]. Specifically, the capacities after 50 cycles are calculated to be 284 mAhg^{-1} , 394 mAhg^{-1} , and 560 mAhg^{-1} with the MPDMS mass ratio of 0.125, 0.50, and 2.0. It can be seen that the increasing mass ratio of MPDMS lifts the capacities of the free carbon matrix. The introduction of MPDMS into the methacrylate network modifies the microstructures of the free carbon matrix. Based on Raman analysis, formation of disordered carbon is promoted by MPDMS, which is capable of storing more lithium ions than ordered carbon [28]. This could be the major reason responsible for the SiOC/C nanohybrid to possess capacities comparable to bare carbon. It is a distinct advantage that reasonable capacities

are achieved with smaller amount of free carbon. It is well accepted that the carbon phase is associated with the formation of dendrite lithium metal during charging process, leading to dramatically increased safety risk. Therefore, reducing the amount of carbon used as the LIB anode while keeping reasonable capacity simultaneously may provide new opportunity to enhance the operation safety of the LIBs.

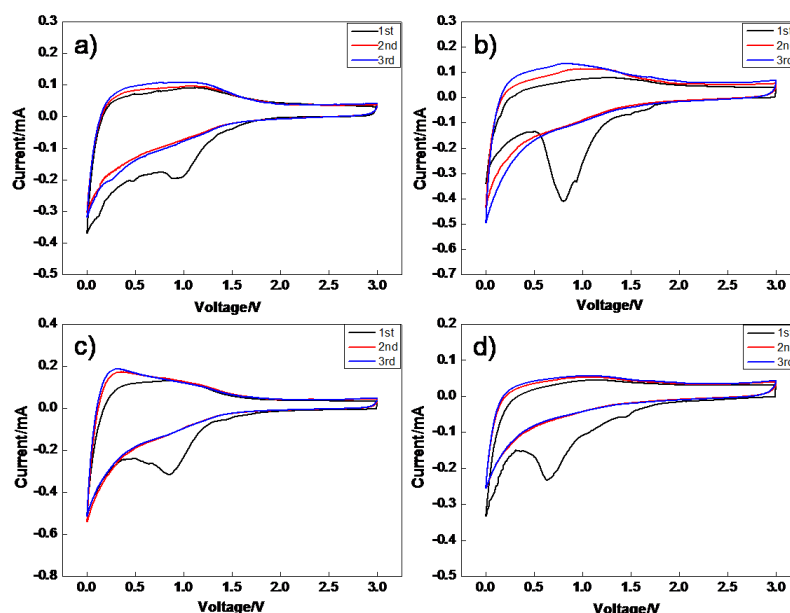


Fig. 9. Cyclic voltammetry curves of the SiOC/C nanohybrids prepared with different mass ratio of MPDMS over the total mass of the resin monomer: (a) 0, (b) 0.125, (c) 0.50 and (d) 2.0.

The rate performance of the SiOC/C nanohybrids is exhibited in Figure 10. When the current density is gradually increased to 2 C ($1\text{ C} = 500\text{ mA g}^{-1}$), the discharge capacities of the SiOC/C nanohybrids are still above 100 mA h g^{-1} , which is comparable to that of the bare carbon anode. It indicates that the incorporation of electrochemically inactive SiOC phase does not deteriorate the rate performance of the free carbon matrix. This is due to the fact that more disordered carbon is formed induced by MPDMS. Disordered carbon has worse electron conductivity than ordered carbon, but it is capable of storing more lithium ions than ordered carbon. As a balance, the SiOC/C nanohybrids still exhibit good rate performance at high current density comparable to the bare carbon anode. Furthermore, after cycles at very high density (five cycles each for 10 C and 20 C), the capacities of the SiOC/C nanohybrid with the MPDMS mass ratio of 2.0 can still be recovered to above 500 mA h g^{-1} , which is 25% higher than that of the bare carbon anode. It further indicates that the SiOC/C nanohybrids have a good cyclic stability due to the stabilization effect brought by the SiOC phase.

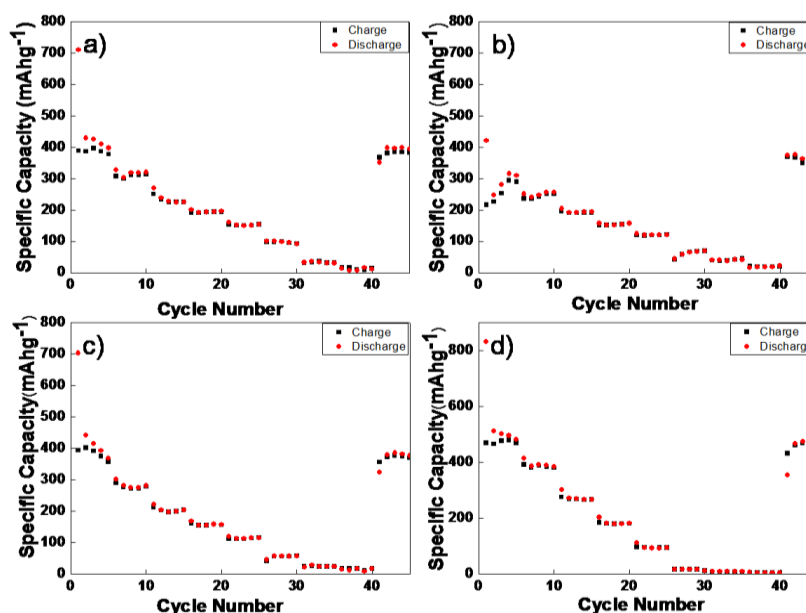


Fig. 10. Rate performance of the SiOC/C nanohybrids prepared with different mass ratio of MPDMS over the total mass of the resin monomer: (a) 0, (b) 0.125, (c) 0.50 and (d) 2.0. The current densities are systematically set at 0.1 C, 0.2 C, 0.5 C, 1.0 C, 2.0 C, 5.0 C, 10 C, 20 C, and 0.1 C (1 C = 500 mA g^{-1}). Five cycles are set for each current density.

4. Conclusions

A facile scalable strategy inspired by dental restorative materials has been developed to synthesize SiOC/C nanohybrids. By adjusting the amount of MPDMS in the resin matrix, the content and microstructure of the free carbon matrix are systematically tuned. SiOC are homogeneously distributed within the free carbon matrix at molecular level and no distinct morphology of the SiOC can be observed. Both the SiOC phase and free carbon are mainly amorphous, where both disordered and ordered carbon exist in the free carbon matrix. Even with less free carbon, good cyclic and rate performance comparable to that of the bare carbon anode are exhibited. This is due to stabilization effect of SiOC and the formation of more disordered carbon induced by MPDMS. Further studies including structure modification to achieve optimized electrochemical performance are in progress and will be presented in the near future.

Acknowledgement

This research is funded by the National Natural Science Foundation of China (51103172), the open project of the Beijing National Laboratory for Molecular Science (20140138), and Ningbo Key Laboratory of Polymer Materials. Donation of the dental resins from Esstech, Inc., USA, is greatly appreciated.

Reference

- [1] M. Li, X.H. Hou, Y.J. Sha, J. Wang, S.J. Hu, X. Liu, Z.P. Shao, *J. Power Sources* **248**, 721 (2014).
- [2] B. Wang, X.L. Li, T.F. Qiu, B. Luo, J. Ning, J. Li, X.F. Zhang, M.H. Liang, L.J. Zhi, *Nano Lett.* **13**, 5578 (2013).
- [3] C.F. Guo, D.L. Wang, T.F. Liu, J.S. Zhu, X.S. Lang, *J. Mater. Chem. A* **2**, 3521 (2014).
- [4] J.O. Besenhard, M. Winter, *ChemPhysChem* **3**, 155 (2002).
- [5] B.-C. Yu, Y. Hwa, J.-H. Kim, H.-J. Sohn, *Electrochim. Acta* **117**, 426 (2014).
- [6] H.C. Tao, X.L. Yang, L.L. Zhang, S.B. Ni, *Mater. Chem. Phys.* **14**, 7528 (2014).
- [7] H. Fukui, H. Ohsuka, T. Hino, K. Kanamura, *J. Electrochem. Soc.* **158**, A550 (2011)
- [8] H. Fukui, H. Ohsuka, T. Hino, K. Kanamura, *J. Power Sources* **196**, 371 (2011).
- [9] N.B. Liao, B.R. Zheng, H.M. Zhou, W. Xue, *J. Mater. Chem. A* **3**, 5067 (2015).
- [10] H. Fukui, Y. Harimoto, M. Akasaka, K. Eguchi, *ACS Appl. Mater. Interfaces* **6**, 12827 (2014).
- [11] A.M. Wilson, G. Zank, K. Eguchi, W. Xing, J.R. Dahn, *J. Power Sources* **68**, 195 (1997).
- [12] R.J.P. Corriu, D. Leclercq, P.H. Mutin, A. Vioux, *J. Sol-Gel Sci. Technol.* **8**, 327 (1997).
- [13] J. Kaspar, M. Graczyk-Zajac, R. Riedel, *J. Power Sources* **244**, 450 (2013).
- [14] J. Kaspar, M. Graczyk-Zajac, R. Riedel, *Solid State Ionics* **225**, 527 (2012).
- [15] P. Colombo, G. Mera, R. Riedel, G.D. Soraru, *J. Am. Ceram. Soc.* **93**, 1805 (2010).
- [16] X. Wang, J.-Q. Meng, M. Wang, Y. Xiao, R. Liu, Y. Xia, Y. Yao, E. Metwalli, Q. Zhang, B. Qiu, Z. Liu, J. Pan, L.-D. Sun, C.-H. Yan, P. Mueller-Buschbaum, Y.-J. Cheng, *ACS Appl. Mater. Interfaces* **7**, 24247 (2015).
- [17] Y. Xiao, X. Wang, Y. Xia, Y. Yao, E. Metwalli, Q. Zhang, R. Liu, B. Qiu, M. Rasool, Z. Liu, J.-Q. Meng, L.-D. Sun, C.-H. Yan, P. Muller-Buschbaum, Y.-J. Cheng, *ACS Appl. Mater. Interfaces* **6**, 18461 (2014).
- [18] Y.J. Cheng, J.M. Antonucci, S.D. Hudson, N.J. Lin, X.R. Zhang, S. Lin-Gibson, *Adv. Mater.* **23**, 409 (2011).
- [19] J. Jung, J. Oh, *Dig. J. Nanomater. Bios.* **9**, 503 (2014).
- [20] A. Matei, M. Zamfirescu, M. Dinescu, E.C. Buruiana, T. Buruiana, A. Lungu, C. Mustaciosu, *Dig. J. Nanomater. Bios.* **7**, 823 (2012).
- [21] F. Tuinstra, J.L. Koenig, *J. Chem. Phys.* **53**, 1126 (1970).
- [22] M.A. Pimenta, G. Dresselhaus, M.S. Dresselhaus, L.G. Cancado, A. Jorio, R. Saito, *Phys. Chem. Chem. Phys.* **9**, 1276 (2007).
- [23] A. Sadezky, H. Muckenhuber, H. Grothe, R. Niessner, U. Poschl, *Carbon* **43**, 1731 (2005).
- [24] M. Graczyk-Zajac, L. Toma, C. Fasel, R. Riedel, *Solid State Ionics* **225**, 522 (2012).
- [25] N. Janakiraman, F. Aldinger, *J. Eur. Ceram. Soc.* **29**, 163 (2009).
- [26] A. Karakuscu, R. Guider, L. Pavesi, G.D. Soraru, *J. Am. Ceram. Soc.* **92**, 2969 (2009).
- [27] P. Dibandjo, M. Graczyk-Zajac, R. Riedel, V.S. Pradeep, G.D. Soraru, *J. Eur. Ceram. Soc.* **32**, 2495 (2012).
- [28] H. Azuma, H. Imoto, S. Yamada, K. Sekai, *J. Power Sources* **81**, 1 (1999).